Weierstraß-Institut
für Angewandte Analysis und Stochastik
Leibniz-Institut im Forschungsverbund Berlin e. V.

Preprint ISSN 2198-5855

H_2-dependent attachment kinetics and shape evolution in chemical vapor deposition graphene growth

Esteban Meca[1, 2], Vivek B. Shenoy[3], John Lowengrub[4]

submitted: December 21, 2016

[1] Department of Mathematics
University of California, Irvine
CA 92697-3875, USA

[2] Weierstrass Institute
Mohrenstr. 39
10117 Berlin
Germany
E-Mail: esteban.mecaalvarez@wias-berlin.de

[3] Department of Materials Science and Engineering
University of Pennsylvania
Philadelphia PA 19104-6272, USA
E-Mail: vshenoy@seas.upenn.edu

[4] Departments of Mathematics
Chemical Engineering & Materials Science
University of California, Irvine
CA 92697-3875, USA
E-Mail: lowengrb@math.uci.edu

No. 2358
Berlin 2016

2010 *Physics and Astronomy Classification Scheme.* 68.43.Jk, 81.10.Aj, 81.15.Aa.

EM acknowledges support from the Balsells foundation and the Einstein Foundation Berlin in the framework of MATHEON. VBS acknowledges partial support from the National Science Foundation through grants CMMI-1311721, DMS-1522603, and DMS-1216801. JL acknowledges partial support from NSF grant DMS-1522775.

Edited by
Weierstraß-Institut für Angewandte Analysis und Stochastik (WIAS)
Leibniz-Institut im Forschungsverbund Berlin e. V.
Mohrenstraße 39
10117 Berlin
Germany

Fax: +49 30 20372-303
E-Mail: preprint@wias-berlin.de
World Wide Web: http://www.wias-berlin.de/

Abstract

Experiments on graphene growth through chemical vapor deposition (CVD) involving methane (CH_4) and hydrogen (H_2) gases reveal a complex shape evolution and a non-monotonic dependence on the partial pressure of H_2 (p_{H_2}). To explain these intriguing observations, we develop a microkinetic model for the stepwise decomposition of CH_4 into mobile radicals and consider two possible mechanisms of attachment to graphene crystals: CH radicals to hydrogen-decorated edges of the crystals and C radicals to bare crystal edges. We derive an effective mass flux and an effective kinetic coefficient, both of which depend on p_{H_2}, and incorporate these into a phase field model. The model reproduces both the non-monotonic dependence on p_{H_2} and the characteristic shapes of graphene crystals observed in experiments. At small p_{H_2}, growth is limited by the kinetics of attachment while at large p_{H_2} growth is limited because the effective mass flux is small. We also derive a simple analytical model that captures the non-monotone behavior, enables the two mechanisms of attachment to be distinguished and provides guidelines for CVD growth of defect-free 2D crystals.

Layers of two-dimensional materials such as graphene and 2D chalcogenides have attracted considerable research interest due to their appealing electrical, optical and mechanical properties [8, 13, 5, 11, 36]. While multiple approaches can be used for synthesis, chemical vapor deposition (CVD) has emerged as the primary method for growing large-area graphene crystals [21, 26] using a combination of gases typically involving hydrogen (H_2) and methane (CH_4), with the latter being the source of carbon. However, CVD is a complex process and growth conditions are largely empirically determined.

CVD involves many mobile radicals stemming from the catalyic decomposition of CH_4 vapor on the surface (e.g., copper), as well as different edge terminations of graphene crystals [38]. Hence attachment and diffusion kinetics play an important role in the growth and morphologies of graphene. Intriguingly, the growth of monolayer graphene islands on copper (Cu) substrates in experiments is found to depend non-monotonously on H_2 pressure [33] (see Fig. 1). However, the role of hydrogen remains unclear [19]. It is believed that hydrogen termination plays a role in the kinetics of attachment and hence in determining the radicals that can attach, e.g., CH or C, [30, 7]. To elucidate the growth mechanisms and provide a rational method for optimizing processing conditions, a unified mathematical model that accounts for all these effects needs to be developed.

Here, we develop a phase field model that accounts for the stepwise decomposition of CH_4 into mobile radicals, the shape of the graphene islands and the structure of graphene edges. To relate the deposition rate with the partial pressures of CH_4 (p_{CH_4}) and H_2 (p_{H_2}), we develop a novel microkinetic model of the catalytic decomposition of CH_4 on Cu substrates. Our main assumption is that H_2 influences the attachment kinetics by attaching to the edge of the graphene layer

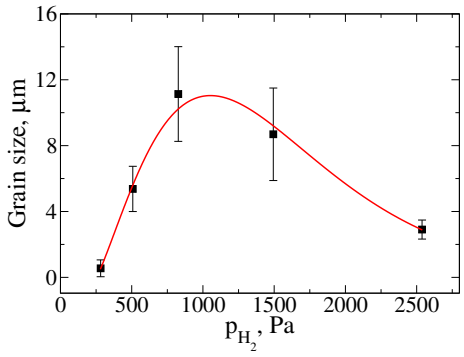

Figure 1: Experimentally-determined non-monotone relation between the sizes of graphene crystals and the hydrogen partial pressure p_{H_2}, adapted from Vlassiouk et al. [33] (with permission).

and facilitating the incorporation of CH radicals to the edge [30]. While recent results suggest that the attaching species is CH [30], we also consider the possibility that C radicals attach directly. We then develop models for the effective flux and kinetic coefficient and incorporate them into the phase field framework.Thus we are able to keep track of the evolving sizes and shapes of the graphene crystals and the abundance and spatial distribution of radicals.

The catalytic decomposition of CH_4 on copper has several stages, see the Appendix and Ref.18 for a detailed description. We assume that the rate-limiting step corresponds to the adsorption and first dehydrogenation of CH_4 on the Cu surface, because of its high activation energy[12]. An analysis of the reactions (see Appendix) shows that the surface coverages of CH radicals (θ_{CH}) and C radicals (θ_{C}) satisfy

$$\frac{d\theta_{\mathsf{CH}}}{dt} = F_{\mathsf{CH}} \equiv \frac{K_1 K_2 k_{AD,\mathsf{CH}_4}}{K_{\mathsf{H}}} \frac{p_{\mathsf{CH}_4}}{p_{\mathsf{H}_2}}, \tag{1a}$$

$$\frac{d\theta_{\mathsf{C}}}{dt} = F_{\mathsf{C}} \equiv \frac{K_1 K_2 K_3 k_{AD,\mathsf{CH}_4}}{K_{\mathsf{H}}^{3/2}} \frac{p_{\mathsf{CH}_4}}{p_{\mathsf{H}_2}^{3/2}}, \tag{1b}$$

where we have disregarded desorption for simplicity (the more general case is given in the Appendix). Here, F_{CH} and F_{C} are fluxes, k_{AD,CH_4} is the rate of adsorption and dehydrogenation of CH_4 and the K_i are equilibrium constants, which are defined in the Appendix. When the attachment of C is considered (e.g., (1b)), we also investigated the possibility that the rate-limiting step is the decomposition of $\mathsf{CH}_{(a)}$ radicals as suggested by the high activation energy of the process [37, 12, 20] (see Appendix). Here, the subscript a denotes ädsorbedßpecies. However, the results lead to the same scaling of F_{C} with p_{CH_4} and p_{H_2} and thus do not qualitatively alter our conclusions below.

The dissociative adsorption of H_2 on the edge leads to the following law for the hydrogen edge coverage $\theta_{\mathsf{H}_{(e)}}$ (see Appendix):

$$\theta_{\mathsf{H}_{(e)}} = \frac{\left(\frac{p_{\mathsf{H}_2}}{p_{\mathsf{H}_2,c}}\right)^{2m}}{1 + \left(\frac{p_{\mathsf{H}_2}}{p_{\mathsf{H}_2,c}}\right)^{2m}}, \tag{2}$$

where $p_{\mathsf{H}_2,c} = K_{\mathsf{H},(e)}^{-1}$ and $K_{\mathsf{H},(e)}$ is the equilibrium constant of the process. The order of reaction

m can have different values. If H_2 adsorption requires two edge sites, then $m = 1/4$, but this is not necessarily the case, hence we treat m as a parameter. In principle, m may be estimated from experimental data or atomistic models.

By using the step transparency approximation [27], we can take the coverages of CH and C as continuous across the graphene edge (see Appendix for the more general case). Also, in this limit there is no distinction between the edge attachment coefficients from the graphene island and substrate, and the edge velocity V is given by (see Appendix):

$$V = \nu_{\mathsf{CH}}(\theta_{\mathsf{CH},\pm} - \theta_{\mathsf{CH},eq}) + \nu_{\mathsf{C}}(\theta_{\mathsf{C},\pm} - \theta_{\mathsf{C},eq}), \tag{3}$$

where ν_{CH} and ν_{C} are the attachment-detachment coefficients, $\theta_{\mathsf{CH},\pm}$ and $\theta_{\mathsf{C},\pm}$ are the coverages close to the step edge and $\theta_{\mathsf{CH},eq}$ and $\theta_{\mathsf{C},eq}$ are the equilibrium concentrations, which incorporate the dependence on the step curvature.

Next, we assume that CH attaches to the edges of the graphene crystal decorated by hydrogen and C attaches to bare edges. This can be modeled as:

$$\nu_{\mathsf{CH}} = \theta_{\mathsf{H}_{(e)}}\nu'_{\mathsf{CH}}, \tag{4}$$

$$\nu_{\mathsf{C}} = (1 - \theta_{\mathsf{H}_{(e)}})\nu'_{\mathsf{C}}, \tag{5}$$

where the primed attachment-detachment coefficients are taken as constants.

Let $\theta_{eff} = \alpha_{\mathsf{CH}}\theta_{\mathsf{CH}} + \alpha_{\mathsf{C}}\theta_{\mathsf{C}}$ be an effective surface coverage and $j_{n,eff,\pm}$ be the associated effective flux: $j_{n,eff,\pm} = \mp\, \hat{n} \cdot D_{eff}\nabla\theta_{eff}|_{\pm} \mp V\theta_{eff,\pm}$. An analysis (see Appendix) shows that these definitions are consistent with the fluxes of the individual species if and only if $\alpha_{\mathsf{CH}} = \alpha_{\mathsf{C}}$ when the diffusion coefficients of the individual species are the same. For convenience we take $\alpha_{\mathsf{CH}} = \alpha_{\mathsf{C}} = 1$, which implies that $D_{eff} = D$, the common diffusion coefficient of both species. Analogously, define the effective kinetic coefficient β_{eff} via the relation $\beta_{eff}V = \theta_{eff} - \theta_{eff,eq}$. This, with the additional assumption that C and CH are in equilibrium on the step edge (see Appendix), $\theta_{\mathsf{C},\pm} = K_{3,(e)}\left(\theta_{\mathsf{H}_{(e)}}^{-1} - 1\right)\theta_{\mathsf{CH},\pm}$, leads together with Eqs. (2), (3), and (5) to the following expression for β_{eff} (see Appendix):

$$\beta_{eff}\nu'_{\mathsf{CH}} = \frac{\left(\left(\frac{p_{\mathsf{H}_2}}{p_{\mathsf{H}_2,c}}\right)^{2m} + K_{3,(e)}\right)\left(1 + \left(\frac{p_{\mathsf{H}_2}}{p_{\mathsf{H}_2,c}}\right)^{2m}\right)}{\left(\frac{p_{\mathsf{H}_2}}{p_{\mathsf{H}_2,c}}\right)^{4m} + (\nu'_{\mathsf{C}}/\nu'_{\mathsf{CH}})K_{3,(e)}} \tag{6}$$

When carbon attachment is unlikely ($\nu'_{\mathsf{CH}} \gg \nu'_{\mathsf{C}}$) and $p_{\mathsf{H}_2}/p_{\mathsf{H}_2,c} \ll 1$, then Eq. (6) can be approximated by:

$$\beta_{eff}\nu'_{\mathsf{CH}} \approx 1 + K_{3,(e)}\left(\frac{p_{\mathsf{H}_2}}{p_{\mathsf{H}_2,c}}\right)^{-4m}. \tag{7}$$

Putting everything together, incorporating kinetic and edge energy anisotropies and nondimensionalizing as in [24], we obtain a Burton-Cabrera-Frank (BCF) type model:

$$\partial_t u = \nabla^2 u + f_{eff}, \tag{8}$$

$$V = \hat{n} \cdot \left(\nabla u|_{+} - \nabla u|_{-}\right), \tag{9}$$

$$u_I = d_0\left(\xi_{e,n}(\psi) + \xi''_{e,n}(\psi)\right)\kappa + \bar{\beta}_{eff}\xi_{k,n}(\psi)V \tag{10}$$

where $u = (\theta_{eff} - \theta_{eff,eq,0})\,\Omega$ and Ω^{-1} is the density of sites on the Cu surface. The nondimensional flux is $f_{eff} = (F_{\mathsf{C}} + F_{\mathsf{CH}})l^2\Omega/D$, where l is an atomic length scale. The parameter d_0 is a nondimensional edge energy and $\xi_{e,n}(\psi)$ and $\xi_{k,n}(\psi)$ are the edge and kinetic anisotropies (normalized such that $\xi_{e,n} = \xi_{k,n} = 1$ in the isotropic case). ψ is the normal angle (angle between the normal vector to the edge and the x-axis) and κ is the edge curvature. The nondimensional kinetic coefficient is $\bar{\beta}_{eff} = \beta_{eff}\Omega D/l$. We take the diffusion to be isotropic, a realistic assumption for many facets and substrates, but the model allows for diffusional anisotropies as well (see [23, 24]).

The values chosen for the equilibrium constants and reaction rates that are used in the definition of f_{eff} are described in detail in the Appendix. The value of the diffusion coefficient has been chosen to give a target value of f_{eff} that gives shapes similar to those observed in experiments. It is within the bounds of the expected values of D, see the Appendix. We have also taken $m = 1$; other choices give similar results (not shown). The kinetic and line energy anisotropies are $\xi_{e,n}(\psi) = 1 + \epsilon_{e,n}\cos(n\psi)$, $\xi_{k,n}(\psi) = 1 + \epsilon_{k,n}\cos(n\psi)$. In order to solve Eqs. (10) we use the phase field model developed in [24] (see Appendix).

Fig. 2 shows the time evolution of the average radius of a crystal, for three different values of p_{H_2}. Starting with an initially circular nucleus with radius $r_0 = 0.3$, the average radius (computed by dividing the area by π and taking the square root) increases smoothly, but for $p_{\mathsf{H}_2} = 1500$ Pa there is a sudden change of slope around $t \approx 0.8$ where the crystal starts growing much more rapidly. The transition is associated with a change from slow growth in the diffusion-limited regime to rapid growth in the kinetic-limited regime (see Figs. S2 and S3 in the Appendix for the behavior with other p_{H_2}). The figure also shows that at late times (after the diffusion-limited to kinetic-limited growth transition) the radius depends non-monotonically on p_{H_2} with slow growth at small and large p_{H_2} and more rapid growth in between. At high p_{H_2}, growth is slow because the flux f_{eff} is small due to the scaling of F_{C} and F_{CH_2} with p_{H_2}, (e.g., Eqs. (1a) and (1b)), which reflects the fact that the enhanced coverage of H_2 decreases the available adsorption sites for CH_4 (see the Appendix). At small p_{H_2} growth is limited by the kinetics of attachment (e.g., Eq. (6)).

The crystallite shapes also vary markedly. While the crystal is mostly circular for $p_{\mathsf{H}_2} = 500$ Pa, $p_{\mathsf{H}_2} = 2000$ Pa and for $p_{\mathsf{H}_2} = 1500$ Pa for $t < 0.8$ (not shown), a complex morphology develops in the latter case for $t > 0.8$. Dendrites grow in the directions in which the kinetic coefficient is the smallest, and develop complex sidebranching patterns that eventually merge, thus creating a large and mostly hexagonal crystallite.

In Fig. 3 we plot the average graphene radii as a function of p_{H_2} at three different times, as labeled. Insets show selected crystallite morphologies (at time t_3). At each time, the crystallite radius is a non-monotonic function of p_{H_2}, as anticipated in Fig. 2. A maximum is clearly found around $p_{\mathsf{H}_2} = 1000$ Pa for $t = t_1$ that moves to around $p_{\mathsf{H}_2} = 1250$ Pa for $t = t_3$. Also, notice how the curve for $t = t_1$ is nearly parabolic before flattening out for $p_{\mathsf{H}_2} > 1500$ Pa, indicating that the effect of p_{H_2} on the radius has saturated. Also, notice how the shapes of the crystallites at $t = t_3$ change with the pressure. The shapes for the lower pressures (e.g. $p_{\mathsf{H}_2} = 750$ Pa) are smoothed six-point stars. As p_{H_2} increases the side branching becomes more and more intense. As the side branches merge together, the overall shape becomes less star-like and more hexagon-like. Note that, for $p_{\mathsf{H}_2} = 1750$ Pa the side branches have not yet merged, but

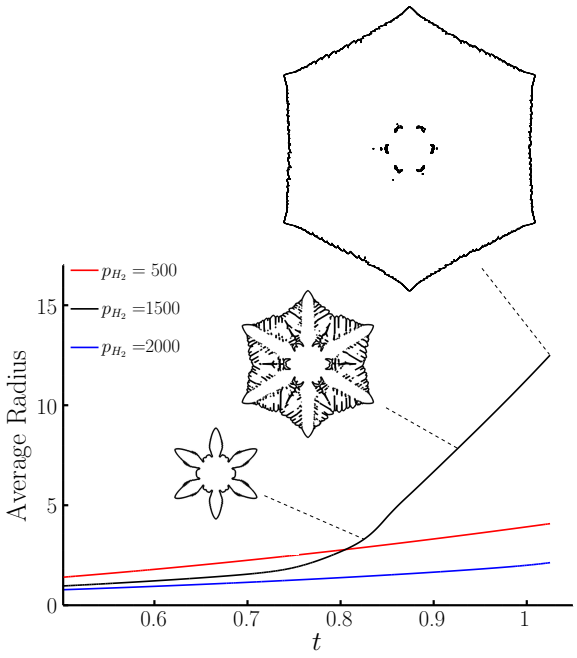

Figure 2: Evolution of the average radius of the crystallites as a function of time for different p_{H_2} as labeled (insets show their shapes). When $p_{\mathrm{H}_2} = 1500$ Pa there is a transition around $t \approx 0.8$ from slow diffusion-limited growth to fast kinetic-limited growth.

they merge at later times to become a shape very close to a hexagon (not shown). These results are consistent with experimental observations [33].

Next, we analyze the transition from the diffusion-limited growth regime to the kinetic-limited regime observed in Fig. 2 in more detail. Since this transition is general and does not depend qualitatively on the anisotropy, we consider the isotropic case and analyze the growth of a circular graphene crystallite. Reformulating Eqs. (8)-(10) in the special case of radial symmetry, it can be seen that the crystallite radius satisfies the boundary integral equation:

$$-\frac{d_0}{r} - \beta_{eff}\dot{r} + f_{eff} \cdot t - \int_0^t \frac{e^{-\frac{r^2+r'^2}{4(t-t')}}}{2(t-t')} I_0\left(\frac{r'r}{2(t-t')}\right) r'\dot{r}'dt' = 0 \tag{11}$$

where $r = r(t)$, $r' = r(t')$, the overdot denotes the time derivative and I_0 is the modified Bessel function of order 0. We have solved numerically Eq. (11) with a simple code based on Chebyschev collocation, for the corresponding numerical parameters of the phase-field model.

In Fig. 4 we present the crystallite radii, as a function of p_{H_2} at several different times, obtained from Eq. (11) using the two different definitions of β_{eff} given in Eqs. (6) and (7). For $p_{\mathrm{H}_2} > 400$ Pa both equations yield similar results and match qualitatively the behavior observed in the phase field simulations shown in Fig. 3. Differences in behaviors arise for smaller values of p_{H_2}. In Fig. 4(left), which corresponds to Eq. (6) where C and CH radicals both may attach to the graphene crystal (see inset), there is a local minimum in the radius around $p_{\mathrm{H}_2} \approx 400$ Pa. As p_{H_2} decreases further, the radius starts to increase due to the attachment of C in this

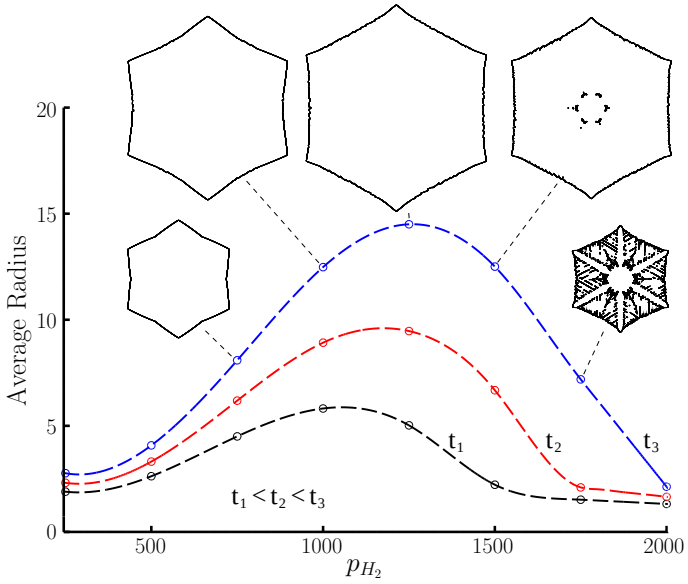

Figure 3: Average graphene crystal radii as a function of p_{H_2} at three different times, as labeled ($t_1 = 0.775$, $t_2 = 0.9$ and $t_3 = 1.025$; insets show shapes at t_3). At each time, the radii depend non-monotonically on p_{H_2}. At low p_{H_2} the crystallites are more star-like while as p_{H_2} increases the shapes become more hexagon-like.

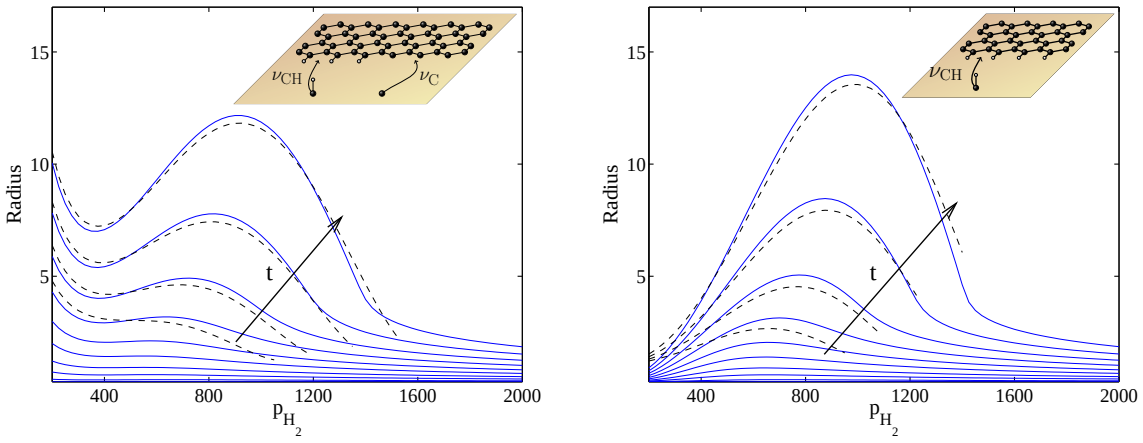

Figure 4: Growth curves obtained from the boundary integral equation (11). The radius (solid) is plotted as a function of p_{H_2} at different times (arrows indicate the direction of increasing time). Left: Both C and CH attach to the growing crystallite (β_{eff} from Eq. 6). Right: only CH attaches (β_{eff} from Eq. 7). A one-parameter fit from (12) is shown with dashed lines. Insets illustrate the attachment mechanisms.

regime where there is little or no H_2 decoration of the interface. A different behavior is observed in Fig. 4(right) where only CH radicals may attach (see inset) and Eq. (7) is used instead. In this case, there is no minimum and the radius decreases to zero as p_{H_2} decreases because the H_2 decoration of the interface, to which CH radicals need to attach, vanishes in this limit. From these results we may conclude: (1) the simple circularly symmetric model (in Eq. (11)) is able to reproduce qualitatively the non-monotone behavior of the average radius curves observed in Fig. 3, and (2) that this model allows us to distinguish between two possible mechanisms of graphene crystallite growth by analyzing the growth behavior at small p_{H_2}. Comparing these results with the experimental results from [33] in Fig. 1 suggests that the experimental results are more consistent with the growth mechanism where only CH attaches at the crystal edge. We return to this point below.

Finally, an analysis of Eq. (11) allows us to find a simple relation for the evolution of the radius in the kinetically-dominated regime, which is the relevant regime for the study of the sizes and shapes of the graphene crystallites at later growth times. It is easy to see that when the $f_{eff} \cdot t$ term in Eq. (11) becomes large enough only the $\beta_{eff}\dot{r}$ term can balance it. This leads to a quadratic relation between the radius and time:

$$r(t) \approx r(0) + \frac{1}{2}\frac{f_{eff}}{\beta_{eff}}\left(t - \frac{1}{f_{eff}}\right)^2, \tag{12}$$

which allows us to define precisely the kinetic-controlled regime. In addition, Eq. (12) enables us to predict the radius of the islands in that regime with surprising accuracy, given the appropriate f_{eff} and β_{eff}. Fig. 4 displays examples of such fits with the radius from Eq. (12) plotted as the dashed curve. For a single value of $r(0)$, independent of p_{H_2} and time, we see that Eq. (12) provides an excellent prediction of behavior of the crystallite radii at moderate-to-small values of p_{H_2}, which is in the kinetic-dominated regime. The flat regions observed at large p_{H_2} correspond to the diffusion-dominated growth regime.

In this study, we developed a microkinetic model to account for the stepwise decomposition of CH_4 into mobile radicals during CVD growth of graphene on Cu substrates. We derived an effective kinetic attachment coefficient, which depends nonmonotonically on p_{H_2}, and an effective mass flux that decreases with p_{H_2}.Using these in a phase field model allowed us to reproduce the complex shape evolution of graphene crystals and the non-monotonic dependence of their sizes on the partial pressure of H_2. A simpler boundary integral model was used to analyze the mechanism behind the non-monotonic growth. In the kinetic regime, we found a simple equation that was capable of accurately reproducing the crystallite radii.

We analyzed two possible mechanisms of attachment. In one mechanism, both C and CH could attach (Eq. (6)) with C attaching to bare graphene edges and CH attaching to hydrogen-decorated edges. In the other, only CH was able to attach to hydrogen-decorated edges and there was no direct C attachment even if edges are bare (Eq. (7)). We found the latter mechanism to be most consistent with experimental results in [33]. However, a recent study [7] found graphene growth at extremely low values of p_{H_2}, and argued that the results observed in [33] were due to the presence of oxidizing impurities. Our approach is capable of accounting for both possibilities and provides a litmus test to distinguish between them. For example, both attachment mechanisms yield similar results for $p_{H_2} > 400$ Pa. However, when both C and CH may attach, we find that the growth of crystallites is still possible for small values of p_{H_2} (Fig. 4).

References

[1] I. Alstrup, I. Chorkendorff, and S. Ullmann. The interaction of CH4 at high temperatures with clean and oxygen precovered Cu(100). *Surface Science*, 264(1–2):95 – 102, 1992. ISSN 0039-6028. doi: http://dx.doi.org/10.1016/0039-6028(92)90168-6. URL http://www.sciencedirect.com/science/article/pii/0039602892901686.

[2] S. Andersson and M. Persson. Crystal-face dependence of physisorption potentials. *Phys. Rev. B*, 48:5685–5688, Aug 1993. doi: 10.1103/PhysRevB.48.5685. URL http://link.aps.org/doi/10.1103/PhysRevB.48.5685.

[3] G. Anger, A. Winkler, and K.D. Rendulic. Adsorption and desorption kinetics in the systems H2/Cu(111), H2/Cu(110) and H2/Cu(100). *Surface Science*, 220(1):1 – 17, 1989. ISSN 0039-6028. doi: http://dx.doi.org/10.1016/0039-6028(89)90459-7. URL http://www.sciencedirect.com/science/article/pii/0039602889904597.

[4] L. W. Bruch, R. D. Diehl, and J. A. Venables. Progress in the measurement and modeling of physisorbed layers. *Rev. Mod. Phys.*, 79:1381–1454, Nov 2007. doi: 10.1103/RevModPhys.79.1381. URL http://link.aps.org/doi/10.1103/RevModPhys.79.1381.

[5] S.Z. Butler, S.M. Hollen, L.Y. Cao, Y. Cui, J.A. Gupta, H.R. Gutierrez, T.F. Heinz, S.S. Hong, J.X. Huang, A.F. Ismach, E. Johnston-Halperin, M. Kuno, V.V. Plashnitsa, R.D. Robinson, R.S. Ruoff, S. Salahuddin, J. Shan, L. Shi, M.G. Spencer, M. Terrones, W. Windl, and J.E. Goldberger. Progress, challenges and opportunities in two-dimensional materials beyond graphene. *ACS Nano*, 7:2898–2926, 2013.

[6] Jin-Ho Choi, Zhancheng Li, Ping Cui, Xiaodong Fan, Hui Zhang, Changgan Zeng, and Zhenyu Zhang. Drastic reduction in the growth temperature of graphene on copper via enhanced london dispersion force. *Sci. Rep.*, 3:–, May 2013. URL http://dx.doi.org/10.1038/srep01925.

[7] Saman Choubak, Pierre L Levesque, Etienne Gaufres, Maxime Biron, Patrick Desjardins, and Richard Martel. Graphene CVD: Interplay between growth and etching on morphology and stacking by hydrogen and oxidizing impurities. *The Journal of Physical Chemistry C*, 118(37):21532–21540, 2014.

[8] Rebecca S Edwards and Karl S Coleman. Graphene synthesis: relationship to applications. *Nanoscale*, 5(1):38–51, 2013.

[9] Y.Y. Fei, P. Thomas, and X.D. Zhu. Adsorption and desorption of hydrogen on bare and xe-covered cu(111). *Applied Physics A*, 86(1):115–121, 2007. ISSN 0947-8396. doi: 10.1007/s00339-006-3742-6. URL http://dx.doi.org/10.1007/s00339-006-3742-6.

[10] Matthias B. Fichtl and Olaf Hinrichsen. On the temperature programmed desorption of hydrogen from polycrystalline copper. *Catalysis Letters*, 144(12):2114–2120, 2014. ISSN 1572-879X. doi: 10.1007/s10562-014-1384-4. URL http://dx.doi.org/10.1007/s10562-014-1384-4.

[11] G. Fiori, F. Bonaccorso, G. Iannaccone, T. Palacios, D. Neumaier, A. Seabaugh, S.K. Banerjee, and L. Colombo. Electronics based on two-dimensional materials. *Nat. Nano.*, 9:768–779, 2014.

[12] Grzegorz Gajewski and Chun-Wei Pao. Ab initio calculations of the reaction pathways for methane decomposition over the cu (111) surface. *J Chem Phys*, 135(6):064707, Aug 2011. doi: 10.1063/1.3624524. URL http://dx.doi.org/10.1063/1.3624524.

[13] A.K. Geim and I.V. Grigorieva. Van der waals heterostructures. *Nature*, 499:419–425, 2013.

[14] Andrew J. Gellman. Oligomer desorption during heterogeneous catalytic synthesis of polymers. *Catalysis Today*, 105(1):144 – 151, 2005. ISSN 0920-5861. doi: http://dx.doi.org/10.1016/j.cattod.2005.04.011. URL http://www.sciencedirect.com/science/article/pii/S0920586105002051.

[15] T. Genger, O. Hinrichsen, and M. Muhler. The temperature-programmed desorption of hydrogen from copper surfaces. *Catalysis Letters*, 59(2-4):137–141, 1999. ISSN 1011-372X. doi: 10.1023/A:1019076722708. URL http://dx.doi.org/10.1023/A%3A1019076722708.

[16] Tu Hu, Qiming Zhang, Jack C. Wells, Xingao Gong, and Zhenyu Zhang. A comparative first-principles study of the adsorption of a carbon atom on copper and nickel surfaces. *Physics Letters A*, 374(44):4563 – 4567, 2010. ISSN 0375-9601. doi: http://dx.doi.org/10.1016/j.physleta.2010.09.022. URL http://www.sciencedirect.com/science/article/pii/S037596011001203X.

[17] A. Karma and W. J. Rappel. Quantitative phase-field modeling of dendritic growth in two and three dimensions. *Phys. Rev. E*, 57(4):4323–4349, 1998.

[18] HoKwon Kim, Eduardo Saiz, Manish Chhowalla, and Cecilia Mattevi. Modeling of the self-limited growth in catalytic chemical vapor deposition of graphene. *New Journal of Physics*, 15:053012, May 2013. doi: 10.1088/1367-2630/15/5/053012.

[19] TPC Klaver, Shou-En Zhu, MHF Sluiter, and GCAM Janssen. Molecular dynamics simulation of graphene on Cu (100) and (111) surfaces. *Carbon*, 82:538–547, 2015.

[20] Kai Li, Chaozheng He, Menggai Jiao, Ying Wang, and Zhijian Wu. A first-principles study on the role of hydrogen in early stage of graphene growth during the CH4 dissociation on Cu(111) and Ni(111) surfaces. *Carbon*, 74:255–265, Aug 2014. ISSN 0008-6223. doi: 10.1016/j.carbon.2014.03.030. URL http://dx.doi.org/10.1016/j.carbon.2014.03.030.

[21] Xuesong Li, Weiwei Cai, Jinho An, Seyoung Kim, Junghyo Nah, Dongxing Yang, Richard Piner, Aruna Velamakanni, Inhwa Jung, Emanuel Tutuc, Sanjay K. Banerjee, Luigi Colombo, and Rodney S. Ruoff. Large-area synthesis of high-quality and uniform graphene films on copper foils. *Science*, 324(5932):1312–1314, June 2009. doi: 10.1126/science.1171245.

[22] Hongyan Liu, Riguang Zhang, Ruixia Yan, Jingrui Li, Baojun Wang, and Kechang Xie. Insight into CH4 dissociation on nicu catalyst: A first-principles study. *Applied Surface Science*, 258(20):8177 – 8184, 2012. ISSN 0169-4332. doi: http://dx.doi.org/10.1016/j.apsusc.2012.05.017. URL http://www.sciencedirect.com/science/article/pii/S0169433212008628.

[23] Esteban Meca, John Lowengrub, Hokwon Kim, Cecilia Mattevi, and Vivek B. Shenoy. Epitaxial graphene growth and shape dynamics on copper: Phase-field modeling and experiments. *Nano Letters*, 13(11):5692–5697, 2013. doi: 10.1021/nl4033928. URL http://pubs.acs.org/doi/abs/10.1021/nl4033928.

[24] Esteban Meca, Vivek B Shenoy, and John Lowengrub. Phase-field modeling of two-dimensional crystal growth with anisotropic diffusion. *Physical Review E*, 88(5):052409, 2013.

[25] Jonathan E. Mueller, Adri C. T. van Duin, and William A. Goddard. Structures, energetics, and reaction barriers for chx bound to the nickel (111) surface. *The Journal of Physical Chemistry C*, 113(47):20290–20306, 2009. doi: 10.1021/jp810555y. URL http://pubs.acs.org/doi/abs/10.1021/jp810555y.

[26] Konstantin S Novoselov, VI Fal, L Colombo, PR Gellert, MG Schwab, K Kim, et al. A roadmap for graphene. *Nature*, 490(7419):192–200, 2012.

[27] O. Pierre-Louis. Phase field models for step flow. *Phys. Rev. E*, 68(2):021604, 2003.

[28] P.B. Rasmussen, P.M. Holmblad, H. Christoffersen, P.A. Taylor, and I. Chorkendorff. Dissociative adsorption of hydrogen on cu(100) at low temperatures. *Surface Science*, 287–288, Part 1(0):79 – 83, 1993. ISSN 0039-6028. doi: http://dx.doi.org/10.1016/0039-6028(93)90746-7. URL http://www.sciencedirect.com/science/article/pii/0039602893907467.

[29] C. T. Rettner, D. J. Auerbach, J. C. Tully, and A. W. Kleyn. Chemical dynamics at the gas–surface interface. *The Journal of Physical Chemistry*, 100(31):13021–13033, 1996. doi: 10.1021/jp9536007. URL http://pubs.acs.org/doi/abs/10.1021/jp9536007.

[30] Nathaniel S. Safron and Michael S. Arnold. Experimentally determined model of atmospheric pressure CVD of graphene on Cu. *J. Mater. Chem. C*, 2:744–755, 2014. doi: 10.1039/C3TC31738B. URL http://dx.doi.org/10.1039/C3TC31738B.

[31] Sung Sakong and Axel Groß. Dissociative adsorption of hydrogen on strained Cu surfaces. *Surface Science*, 525(1–3):107 – 118, 2003. ISSN 0039-6028. doi: http://dx.doi.org/10.1016/S0039-6028(02)02550-5. URL http://www.sciencedirect.com/science/article/pii/S0039602802025505.

[32] J. Tabatabaei, B.H. Sakakini, M.J. Watson, and K.C. Waugh. The detailed kinetics of the adsorption of hydrogen on polycrystalline copper studied by reactive

frontal chromatography. *Catalysis Letters*, 59(2-4):151–155, 1999. ISSN 1011-372X. doi: 10.1023/A:1019028806778. URL http://dx.doi.org/10.1023/A%3A1019028806778.

[33] Ivan Vlassiouk, Murari Regmi, Pasquale F. Fulvio, Sheng Dai, Panos Datskos, Gyula Eres, and Sergei Smirnov. Role of hydrogen in chemical vapor deposition growth of large single-crystal graphene. *Acs Nano*, 5(7):6069–6076, July 2011. doi: 10.1021/nn201978y.

[34] D.-H. Wei, D. C. Skelton, and S. D. Kevan. Lateral interactions and corrugation in physisorption systems: CH4/Cu(100). *The Journal of Chemical Physics*, 105(17):7808–7814, 1996. doi: http://dx.doi.org/10.1063/1.472562. URL http://scitation.aip.org/content/aip/journal/jcp/105/17/10.1063/1.472562.

[35] Steven Wise, Junseok Kim, and John Lowengrub. Solving the regularized, strongly anisotropic cahn-hilliard equation by an adaptive nonlinear multigrid method. *Journal of Computational Physics*, 226(1):414 – 446, 2007. ISSN 0021-9991. doi: DOI:10.1016/j.jcp.2007.04.020. URL http://www.sciencedirect.com/science/article/B6WHY-4NNYJGC-1/2/d7ffb0d68512ab361f9376d49cfd4cd2.

[36] O.V. Yazyev and Y.P. Chen. Polycrystalline graphene and other two-dimensional materials. *Nature Nano.*, 9:755–767, 2014.

[37] Wenhua Zhang, Ping Wu, Zhenyu Li, and Jinlong Yang. First-principles thermodynamics of graphene growth on cu surfaces. *The Journal of Physical Chemistry C*, 115(36):17782–17787, 2011. doi: 10.1021/jp2006827. URL http://pubs.acs.org/doi/abs/10.1021/jp2006827.

[38] Xianfeng Zhang, Jing Ning, Xianglong Li, Bin Wang, Long Hao, Minghui Liang, Meihua Jin, and Linjie Zhi. Hydrogen-induced effects on the CVD growth of high-quality graphene structures. *Nanoscale*, 5:8363–8366, 2013. doi: 10.1039/C3NR01599H. URL http://dx.doi.org/10.1039/C3NR01599H.

Appendix

A Phase field model

In order to solve the BCF model (Eqs. 8-10) we use the phase field model developed in [24]. The phase field variable ϕ, where $\phi \approx 1$ marks the graphene crystal domain, evolves according to

$$\begin{aligned}\alpha\tau(\Theta)\epsilon^2\partial_t\phi &= \epsilon^2\nabla\cdot[\xi_{e,n}(\Theta)^2\nabla\phi] - f'(\phi) + \epsilon\lambda g'(\phi)u \\ &- \epsilon^2\partial_x\left(\xi_{e,n}(\Theta)\xi'_{e,n}(\Theta)\partial_y\phi\right) + \epsilon^2\partial_y\left(\xi_{e,n}(\Theta)\xi'_{e,n}(\Theta)\partial_x\phi\right), \end{aligned} \tag{13}$$

where α is a parameter, ϵ is the edge (interface) thickness, $\tau(\Theta)$ is related to the kinetic anisotropy, see below. The angle Θ defined as $\tan\Theta = \partial_y\phi/\partial_x\phi$. The functions f and g are defined as $f(\phi) = \phi^2(1-\phi)^2/4$, $g(\phi) = \phi^3(10 - 15\phi + 6\phi^2)/120$. The parameter λ is a coupling constant for the diffusion field u_ϵ, which satisfies

$$\partial_t u_\epsilon = \nabla^2 u_\epsilon + f_{eff} - \partial_t \phi. \tag{14}$$

The method of matched asymptotic expansions [17, 24] can be used to show that the BCF Eqs. (8)-(10) are recovered in the limit $\epsilon \to 0$ with second order accuracy (in ϵ) from the phase field model if we take $\lambda = a_1/d_0$, $\alpha = \bar{\beta}_{eff}/d_0$, and $\tau(\Theta) = \xi_{e,n}(\Theta)\xi_{k,n}(\Theta) + \epsilon\, a_2\xi_{e,n}(\Theta)^2/\bar{\beta}_{eff}$, where $a_1 = 10\sqrt{2}$, $a_2 = 47\sqrt{2}/60$. The phase field equations are discretized in space using a block-structured adaptive finite difference method and we use an implicit Crank-Nicolson scheme in time. The discrete equations are solved using the nonlinear adaptive multigrid algorithm developed by Wise et al. [35].

The phase-field parameters ($\epsilon = 2.5 \times 10^{-3}$, $d_0 = 6 \times 10^{-4}$) are the same as those in [24] as are anisotropies ($\epsilon_{k,6} = 0.08$ $\epsilon_{e,6} = 0.001$), and the length scale $l = 10^{-6}m$. We use up to eight levels of refinement for the multigrid, with the finest mesh having a spacing $\Delta x = 0.00195$. See also Table 7.

B Chemical Reactions and Alternative Limiting Step

We take the following reactions as an idealization of the dehydrogenation process of methane [18].

$$\mathrm{CH_{4(g)}} + 2\,\mathrm{S} \underset{k_{D,\mathrm{CH_3}}}{\overset{k_{AD,\mathrm{CH_4}}}{\rightleftharpoons}} \mathrm{CH_{3(a)}} + \mathrm{H_{(a)}} \tag{15}$$

$$\mathrm{CH_{3(a)}} + \mathrm{S} \underset{k_{-,\mathrm{CH_2}}}{\overset{k_{+,\mathrm{CH_3}}}{\rightleftharpoons}} \mathrm{CH_{2(a)}} + \mathrm{H_{(a)}} \tag{16}$$

$$\mathrm{CH_{2(a)}} + \mathrm{S} \underset{k_{-,\mathrm{CH}}}{\overset{k_{+,\mathrm{CH_2}}}{\rightleftharpoons}} \mathrm{CH_{(a)}} + \mathrm{H_{(a)}} \tag{17}$$

$$\mathrm{CH_{(a)}} + \mathrm{S} \underset{k_{-,\mathrm{C}}}{\overset{k_{+,\mathrm{CH}}}{\rightleftharpoons}} \mathrm{C_{(a)}} + \mathrm{H_{(a)}} \tag{18}$$

$$\mathrm{H_{2(g)}} + 2\,\mathrm{S} \underset{k_{D,\mathrm{H}}}{\overset{k_{AD,\mathrm{H_2}}}{\rightleftharpoons}} 2\,\mathrm{H_{(a)}} \tag{19}$$

where S represents an adsorption site on the copper surface.

The kinetics of the previous reactions can be described by the following equations:

$$\frac{d\theta_{\mathrm{CH_3}}}{dt} = k_{AD,\mathrm{CH_4}} p_{\mathrm{CH_4}} (1-\theta)^2 - k_{D,\mathrm{CH_3}} \theta_{\mathrm{CH_3}} \theta_{\mathrm{H}}, \tag{20}$$

$$\frac{d\theta_{\mathrm{CH_2}}}{dt} = k_{+,\mathrm{CH_3}} \left[\theta_{\mathrm{CH_3}} (1-\theta) - K_1^{-1} \theta_{\mathrm{CH_2}} \theta_{\mathrm{H}}\right], \tag{21}$$

$$\frac{d\theta_{\mathrm{CH}}}{dt} = k_{+,\mathrm{CH_2}} \left[\theta_{\mathrm{CH_2}} (1-\theta) - K_2^{-1} \theta_{\mathrm{CH}} \theta_{\mathrm{H}}\right], \tag{22}$$

$$\frac{d\theta_{\mathrm{C}}}{dt} = k_{+,\mathrm{CH}} \left[\theta_{\mathrm{CH}} (1-\theta) - K_3^{-1} \theta_{\mathrm{C}} \theta_{\mathrm{H}}\right], \tag{23}$$

$$\frac{d\theta_{\mathrm{H}}}{dt} = k_{AD,\mathrm{H_2}} \left[p_{\mathrm{H_2}} (1-\theta)^2 - K_{\mathrm{H}}^{-1} \theta_{\mathrm{H}}^2\right], \tag{24}$$

where $\theta = \theta_{\mathrm{CH_3}} + \theta_{\mathrm{CH_2}} + \theta_{\mathrm{CH}} + \theta_{\mathrm{C}} + \theta_{\mathrm{H}}$ is the total coverage, assumed to be small in the following. We define the equilibrium constants in the following way: $K_1 = k_{+,\mathrm{CH_3}}/k_{-,\mathrm{CH_2}}$, $K_2 = k_{+,\mathrm{CH_2}}/k_{-,\mathrm{CH}}$, $K_3 = k_{+,\mathrm{CH}}/k_{-,\mathrm{C}}$ and $K_{\mathrm{H}} = k_{AD,\mathrm{H_2}}/k_{D,\mathrm{H}}$.

B.1 Simplifications

B.1.1 CH Attachment

If we assume that, according to recent studies [30], CH is diffusing and attaching directly to graphene and hence we disregard equation (23), if we take $k_{AD,\mathrm{H_2}} p_{\mathrm{H_2}} \gg k_{AD,\mathrm{CH_4}} p_{\mathrm{CH_4}}$, $k_{+,\mathrm{CH_3}} \gg k_{AD,\mathrm{CH_4}} p_{\mathrm{CH_4}}$, $k_{+,\mathrm{CH_2}} \gg k_{AD,\mathrm{CH_4}} p_{\mathrm{CH_4}}$, given the comparatively small activation energies, and if in addition we take $\theta \ll 1$, i.e., we take a small coverage, then we can put together the previous equations in the following form:

$$\frac{d\theta_{\mathrm{CH}}}{dt} = \frac{K_1 K_2 k_{AD,\mathrm{CH_4}}}{K_{\mathrm{H}}} \frac{p_{\mathrm{CH_4}}}{p_{\mathrm{H_2}}} - k_{D,\mathrm{CH_3}} \sqrt{K_{\mathrm{H}} p_{\mathrm{H_2}}}\, \theta_{\mathrm{CH}} \tag{25}$$

Note that the previous equation follows from considering that $\theta_{\mathrm{CH_2}}$, θ_{CH}, and θ_{H} are *fast* variables, and $\theta_{\mathrm{CH_3}}$ has *slow* dynamics. This leads to a relation of proportionality between θ_{CH} and $\theta_{\mathrm{CH_3}}$ which permits rewriting Eq. (20) as Eq. (25).

If we accept that CH is the diffusing species, then we can make the following identifications:

$$F_{\mathrm{CH}} = \frac{1}{\Omega} \frac{K_1 K_2 k_{AD,\mathrm{CH_4}}}{K_{\mathrm{H}}} \frac{p_{\mathrm{CH_4}}}{p_{\mathrm{H_2}}}, \tag{26}$$

$$\tau = \frac{1}{k_{D,\mathrm{CH_3}} \sqrt{K_{\mathrm{H}} p_{\mathrm{H_2}}}}, \tag{27}$$

where Ω is an average area per atom in the low-index surfaces of copper [10]. We will take $\tau \to \infty$ and hence disregard desorption.

Hence, the non-dimensional deposition rate $f = l^2 F_{\mathrm{CH}} \Omega / \bar{D}$ will be proportional to the ratio of the partial pressures $r = p_{\mathrm{CH_4}}/p_{\mathrm{H_2}}$.

B.1.2 C Attachment

If we assume now that it is C what is diffusing and attaching to graphene, and again we take CH_4 adsorption and first dehydrogenation as the time-limiting process then $k_{AD,\mathrm{H}_2} p_{\mathrm{H}_2} \gg k_{AD,\mathrm{CH}_4} p_{\mathrm{CH}_4}$, $k_{+,\mathrm{CH}_3} \gg k_{AD,\mathrm{CH}_4} p_{\mathrm{CH}_4}$, $k_{+,\mathrm{CH}_2} \gg k_{AD,\mathrm{CH}_4} p_{\mathrm{CH}_4}$, $k_{+,\mathrm{CH}} \gg k_{AD,\mathrm{CH}_4} p_{\mathrm{CH}_4}$. This assumption is made to keep the model as simple as possible. For CH attachment the assumption was done on the basis of very different activation energies, but this is not the case for C attachment[1]. See this section below for an alternate assumption. With the assumptions above, the equation for C kinetics takes then the following form for small coverage:

$$\frac{d\theta_{\mathrm{C}}}{dt} = \frac{K_1 K_2 K_3 k_{AD,\mathrm{CH}_4}}{K_{\mathrm{H}}^{3/2}} \frac{p_{\mathrm{CH}_4}}{p_{\mathrm{H}_2}^{3/2}} - k_{D,\mathrm{CH}_3} \sqrt{K_{\mathrm{H}} p_{\mathrm{H}_2}} \theta_{\mathrm{C}} \tag{28}$$

Note that, as with (28) the previous equation follows from considering that θ_{CH_2}, θ_{CH}, θ_{C}, and θ_{H} are *fast* variables, and θ_{CH_3} has *slow* dynamics. This leads to a relation of proportionality between θ_{C} and θ_{CH_3} which permits rewriting Eq. (20) as Eq. (28).

If we accept that atomic C is the diffusing and attaching species, then we can make the following identifications:

$$F_{\mathrm{C}} = \frac{1}{\Omega} \frac{K_1 K_2 K_3 k_{AD,\mathrm{CH}_4}}{K_{\mathrm{H}}^{3/2}} \frac{p_{\mathrm{CH}_4}}{p_{\mathrm{H}_2}^{3/2}}, \tag{29}$$

$$\tau = \frac{1}{k_{D,\mathrm{CH}_3} \sqrt{K_{\mathrm{H}} p_{\mathrm{H}_2}}}. \tag{30}$$

As in the case of CH, we take $\tau \to \infty$ and hence disregard desorption.

Hence, $f = l^2 F_{\mathrm{C}} \Omega / \bar{D}$ it is not proportional to the ratio of the partial pressures $r = p_{\mathrm{CH}_4} / p_{\mathrm{H}_2}$ anymore.

Alternate assumption If we consider CH dissociation the limiting step, a similar equation can be derived, by assuming $k_{AD,\mathrm{CH}_4} p_{\mathrm{CH}_4} \gg k_{+,\mathrm{CH}}$. Following these new assumptions we arrive to the following analogue of Eq. (28):

$$\frac{d\theta_{\mathrm{C}}}{dt} = \frac{k_{+,\mathrm{CH}} k_{AD,\mathrm{CH}_4} K_1 K_2}{k_{D,\mathrm{CH}_3} K_{\mathrm{H}}^{3/2}} \frac{p_{\mathrm{CH}_4}}{p_{\mathrm{H}_2}^{3/2}} - \frac{k_{+,\mathrm{CH}}}{K_3} \sqrt{K_{\mathrm{H}} p_{\mathrm{H}_2}} \theta_{\mathrm{C}}. \tag{31}$$

This equation leads to the following definitions (tildes denote the different limiting process):

$$F'_{\mathrm{C}} = \frac{1}{\Omega} \frac{k_{+,\mathrm{CH}} k_{AD,\mathrm{CH}_4} K_1 K_2}{k_{D,\mathrm{CH}_3} K_{\mathrm{H}}^{3/2}} \frac{p_{\mathrm{CH}_4}}{p_{\mathrm{H}_2}^{3/2}}, \tag{32}$$

$$\tau' = \frac{K_3}{k_{+,\mathrm{CH}} \sqrt{K_{\mathrm{H}} p_{\mathrm{H}_2}}}. \tag{33}$$

Note that the dependency on $p_{\mathrm{CH}_4} / p_{\mathrm{H}_2}^{3/2}$ is the same as in Eq. (29).

[1] The activation energy of CH dissociation is of the same order as that of CH_4 first dehydrogenation [37, 12].

Parameter	*Value*	*Source*
p_{CH_4}	4 Pa	
K_1	4.23×10^{-4}	[20]
K_2	1.29×10^{-2}	[20]
K_3	6.41×10^{-7}	[20]
K_{H}	3.05×10^{-10} Pa^{-1}	see text
$K_{3,(e)}$	6.0×10^{-7}	fitted
$K_{\mathrm{H},(e)}$	3.8×10^{-7} Pa^{-1}	fitted
k_{AD,CH_4}	2.78×10^{-4} $\mathrm{s}^{-1}\mathrm{Pa}^{-1}$	see text
D	1.79×10^{-14} $\mathrm{m}^2\mathrm{s}^{-1}$	fitted
$\nu'_{\mathrm{CH}}/\nu'_{\mathrm{C}}$	10^9	fitted
$\rho_s\,(\Omega^{-1})$	$1.47{\times}10^{19}$ m^{-2}	[10]

Table 1: Summary of the values of the numerical parameters.

C Numerical Parameters

In this section we discuss the different options considered for the parameters. In Table 1 we show the value of the parameters chosen and their sources.

C.0.3 CH Attachment

By using the different coefficients and equilibrium constants estimated in Appendix D together with K_1K_2 estimated from transition state theory, we can approximate F_{CH} from equation (26) as follows:

$$F_{\mathrm{CH}} = 1.6936 \times 10^{19} \frac{p_{\mathrm{CH}_4}}{p_{\mathrm{H}_2}} \left(\mathrm{m}^{-2}\mathrm{s}^{-1}\right). \tag{34}$$

With Li et al. [20] data for K_1 and K_2, we obtain

$$F_{\mathrm{CH},alt} = 7.31947 \times 10^{19} \frac{p_{\mathrm{CH}_4}}{p_{\mathrm{H}_2}} \left(\mathrm{m}^{-2}\mathrm{s}^{-1}\right), \tag{35}$$

which is about four times higher. Note that we do not use their data for the equilibrium of CH_4 and CH_3, as we assume that adsorption is dissociative and take the experimental data for the dissociative adsorption coefficient.

In order to recover the numerical parameter f we need an estimate of the diffusion coefficient for CH. We can approximate it in the usual way from transition state theory:

$$\bar{D} \approx \Omega\nu \mathrm{e}^{-\frac{E_{diff,\mathrm{CH}}}{kT}}, \tag{36}$$

where we take Ω as the distance between adsorption sites squared. We can approximate ν from the Cu-C vibration frequency which gives $\nu = 1.73 \times 10^{13}\,\mathrm{s}^{-1}$.

The most problematic quantity is the height of the diffusion barrier, $E_{diff,\mathrm{CH}}$, as its value it is unavailable and it can change wildly depending on the Cu surface. We can nevertheless

approximate it. For C atoms on Cu(111) it has been found to be $E_{diff,\mathrm{C}} = 0.09$ eV [16]. We would expect the value of the diffusion barrier to be a bit lower for CH, as the binding energy with the substrate is also lower, this is the case in the CH_x/Ni(111) system [25]. This number gives the following value of the diffusion coefficient:

$$\bar{D}_{(111)} = 5.26 \times 10^{-7}\,\mathrm{m^2 s^{-1}} \tag{37}$$

We can proceed in a similar way for the Cu(100) face. Again from [16], we have that $E_{diff,\mathrm{C}} = 2.12$ eV, which gives the following value of the diffusion coefficient, assuming that the other parameters do not change much:

$$\bar{D}_{(100)} = 7.07 \times 10^{-15}\,\mathrm{m^2 s^{-1}} \tag{38}$$

We see that the two results are very different, with a jump of eight orders of magnitude between the two. This gives the following two values of f:

$$f_{(111)} = \frac{F\,l^2\Omega}{\bar{D}_{(111)}} = 2.19 \times 10^{-6}\frac{p_{\mathrm{CH_4}}}{p_{\mathrm{H_2}}}, \tag{39}$$

$$f_{(100)} = \frac{F\,l^2\Omega}{\bar{D}_{(100)}} = 162\frac{p_{\mathrm{CH_4}}}{p_{\mathrm{H_2}}}, \tag{40}$$

where we take $l = 10^{-6}$ m. We observe a variation of 8 orders of magnitude, which probably means that our method for estimating the diffusion coefficient based in transition state theory or the barrier energies are not correct for CH/Cu.

Taking the values of the equilibrium constants from Li et al. [20], we obtain an analogously large difference between both values of f:

$$f_{(111),alt} = \frac{F_{\mathrm{CH},alt}\,l^2\Omega}{\bar{D}_{(111)}} = 9.47 \times 10^{-6}\frac{p_{\mathrm{CH_4}}}{p_{\mathrm{H_2}}}, \tag{41}$$

$$f_{(100),alt} = \frac{F_{\mathrm{CH},alt}\,l^2\Omega}{\bar{D}_{(100)}} = 704\frac{p_{\mathrm{CH_4}}}{p_{\mathrm{H_2}}}, \tag{42}$$

C.0.4 C Attachment

Similarly, we can compute all the previous numbers for C attachment, using the two approximations discussed, for Cu(111):

$$F_{\mathrm{C}} = 1.83 \times 10^{18}\frac{p_{\mathrm{CH_4}}}{p_{\mathrm{H_2}}^{3/2}}\ \left(\mathrm{m^{-2}s^{-1}}\right), \tag{43}$$

$$F'_{\mathrm{C}} = 2.30 \times 10^{20}\frac{p_{\mathrm{CH_4}}}{p_{\mathrm{H_2}}^{3/2}}\ \left(\mathrm{m^{-2}s^{-1}}\right), \tag{44}$$

and with Li et al. [20] data,

$$F_{\mathrm{C},alt} = 2.68 \times 10^{18}\frac{p_{\mathrm{CH_4}}}{p_{\mathrm{H_2}}^{3/2}}\ \left(\mathrm{m^{-2}s^{-1}}\right), \tag{45}$$

$$F'_{\mathrm{C},alt} = 1.20 \times 10^{19}\frac{p_{\mathrm{CH_4}}}{p_{\mathrm{H_2}}^{3/2}}\ \left(\mathrm{m^{-2}s^{-1}}\right). \tag{46}$$

With the assumptions that the diffusion coefficients are similar, we would obtain values for the reduced deposition coefficients (f) with prefactors of the same order of magnitude than Eqs. (39) and (40).

D Estimating the Model Parameters

We find most of the parameters from experiments and from DFT calculations, in a similar way as Kim et al. [18]. In this section we give a short overview of the problem of determining the adsorption energies, and in the following sections we will go in the detail of our choice.

The adsorption (physisorption) energy for CH_4 comes from [34] (the adsorption energy is equated with the desorption energy, assuming a negligible adsorption barrier, as it is common [4, 14]). The same applies for the physisorption energy of H_2, obtained from Andersson and Persson [2]. The physisorption values are very small and hence we will ignore it, in favor of experimental calculations of the dissociative adsorption.

The energy barrier of dissociative adsorption for H_2 is not well defined as it depends on the particular rotational and vibrational state of the molecule that it is attaching, and hence it depends on temperature in a way much more complex than an Arrhenius law [29]. The variation found goes from $0.3 - 0.8$ eV. Kim et al. [18] use the data from Tabatabaei et al. [32], who reported $E_{b,\mathrm{H}_2} = 0.44$ eV for polycrysralline copper supported on alumina. For unsupported Cu Rasmussen et al. [28] reported $E_{b,\mathrm{H}_2} = 0.50$ eV for the (100) face of Cu, but both of these results are low temperature ($T \approx 250$K). The latter value is consistent with the value computed theoretically by Sakong and Groß [31].

We take the dissociative desorption data for H_2 from [15, 9], together with the prefactor. We have compared also with the values given by Tabatabaei et al. [32], which is the source for the dissociation enthalpy of H_2 on Cu, $\Delta H_{\mathrm{H}_2 \to \mathrm{H+H}} = -0.27$ eV, which is also consistent with theoretical values from Sakong and Groß [31], who report values of -0.21 eV and -0.35 eV for the Cu(100) and Cu(111) faces, respectively. The activation energies for each of the intermediate species CH_x come from [37], [12] and [22]. A summary of all the considered energies and enthalpies is given in Table 2.

D.1 Hydrogen Adsorption/Desorption

The rate of Hydrogen adsorption is modeled as follows:

$$k_{AD,\mathrm{H}_2} = \frac{2\Omega}{\sqrt{2\pi m_{\mathrm{H}_2} kT}} s_0 f(\theta) \exp\left(\frac{-E_{b,\mathrm{H}_2}}{kT}\right), \tag{47}$$

where k is Boltzmann's constant, m_{H_2} is the mass of the molecule, $s_0 f(\theta)$ is the sticking pre-exponential factor, which depends on the coverage ($f(0) = 1$). We take the Langmuir form $f(\theta) = (1-\theta)^2$. Note the factor 2 in the numerator due to the second order kinetics. These parameters can be found in Tabatabaei et al. [32], they are listed in Table 3.

Paramenter	*Symbol*	*Value*(eV)
Adsorption Energy of CH_4 on Cu	$E_{ad,\mathrm{CH_4}}$	-0.165
Physisorption Energy of H_2 on Cu	$E_{ad,\mathrm{H_2}}$	-0.03
Energy Barrier Dissociative Adsorption $H_2 \rightarrow 2\,H$	$E_{b,\mathrm{H_2}}$	0.3-0.8
Energy Barrier Associative Desorption $2\,H \rightarrow H_2$	$E_{des,\mathrm{H}}$	0.63 [9]
Energy Barrier Associative Desorption $2\,H \rightarrow H_2$	$E_{des,\mathrm{H}}$	0.81 [15]
Dissociation Enthalpy of H_2 on Cu	$\Delta H_{\mathrm{H_2 \rightarrow H+H}}$	-0.3
Enthalpy of reaction of $CH_{3,a}$ from $CH_{4,a}$	$\Delta H_{\mathrm{CH_4 \rightarrow CH_3+H}}$	0.75
Enthalpy of reaction of $CH_{2,a}$ from $CH_{3,a}$	$\Delta H_{\mathrm{CH_3 \rightarrow CH_2+H}}$	0.83
Enthalpy of reaction of CH_a from $CH_{2,a}$	$\Delta H_{\mathrm{CH_2 \rightarrow CH+H}}$	0.41

Table 2: Summary of the values of the barrier energies and reaction enthalpies.

Symbol	*Value*	*Units*
s_0	0.0198	–
$E_{b,\mathrm{H_2}}$	0.44	eV

Table 3: H_2 adsorption parameters from Tabatabaei et al. [32].

For the rate of Hydrogen desorption we take the following:

$$k_{D,\mathrm{H}} = \nu_{d0} \exp\left(\frac{-E_{des,\mathrm{H_2}}}{kT}\right) \theta_{\mathrm{H}}^2, \tag{48}$$

where ν_{d0} is the prefactor rate coefficient, with dimensions of frequency.

We have found two sets of parameters for the previous equation. Fei et al. [9] results for H_2 desorption from Cu(111) (Table 4) and Genger et al. [15] together with Anger et al. [3] (Table 5).

The values from Table 5 depend on the coverage and are more in line with other calculations, and hence we will keep them. They imply the following values of $k_{D,\mathrm{H}}$ and $k_{AD,\mathrm{H_2}}$:

$$k_{AD,\mathrm{H_2}} = 0.0879\,\mathrm{Pa^{-1}s^{-1}} \tag{49}$$

$$k_{D,\mathrm{H}} = 2.885 \times 10^8\,\mathrm{s^{-1}} \tag{50}$$

Symbol	*Value*	*Units*
ν_{d0}	1×10^9	s^{-1}
$E_{des,\mathrm{H_2}}$	0.63	eV

Table 4: H_2 desorption parameters from Fei et al. [9].

Symbol	*Value*	*Units*
ν_{d0}	3×10^{11}	s^{-1}
E_{des,H_2}	0.78	eV

Table 5: H_2 desorption parameters from Genger et al. [15] and Anger et al. [3].

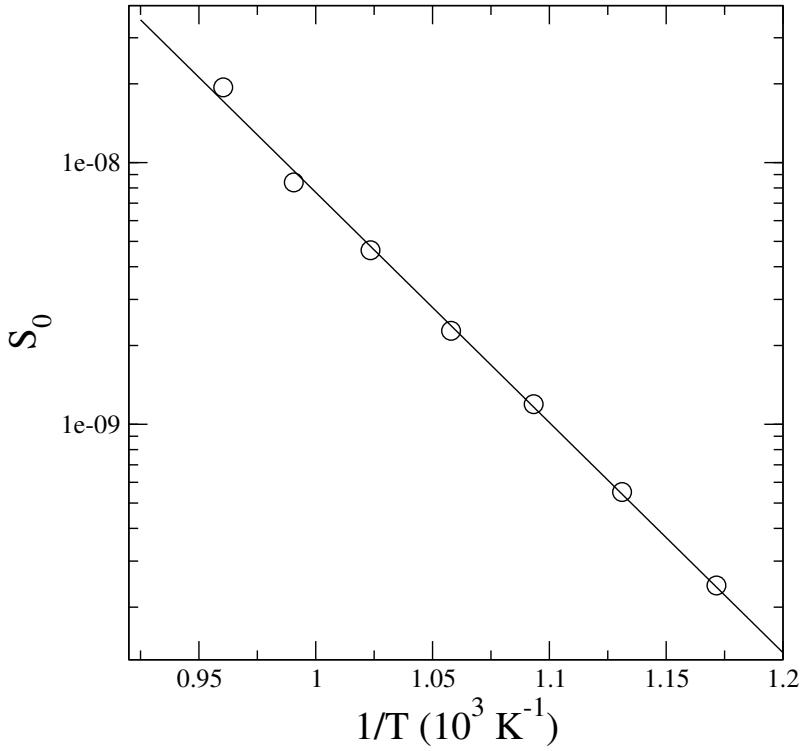

Figure 5: Initial sticking coefficient for CH_4 on Cu(100) (figure recreated from [1] using g3data)

D.2 Methane and CH_x microkinetics

The values of k_{AD,CH_4} and k_{D,CH_3} can be approximated in a similar way to those of H_2, but the equilibrium constants K_1, K_2, and K_3 remain unknown due to the unknown ratio of the exponential prefactors. We take their value from [20].

In order to obtain k_{AD,CH_4} we need the initial sticking coefficient. We have recovered the data from Alstrup et al. [1] for CH_4/Cu(100) (see Fig. 5) and then by fitting an Arrhenius law, we have obtained the values in Table 6.

Symbol	*Value*	*Units*
s_0	4.79	–
E_{b,CH_4}	1.75	eV

Table 6: Parameters for CH_4 adsorption from [1] (see Fig. 5).

The barrier energy from Table 6 is in good agreement with [37] ($E_b = 1.77$ eV for Cu(100)) and it is somewhat larger than the value for the Cu(111) surface, $E_b = 1.59$ eV [37] and $E_b = 1.57$ eV [12].

We will take $E_{b,\mathrm{CH_4}} = 1.59$ eV and $s_0 = 5$. It is common to arbitrarily take the value $s_0 = 1$ [6, 18], but in light of the previous experimental result, $s_0 = 5$ is probably a more realistic choice. With this value, the expected value of $k_{AD,\mathrm{CH_4}}$ is:

$$k_{AD,\mathrm{CH_4}} = \frac{2\Omega}{\sqrt{2\pi m_{\mathrm{CH_4}} kT}} s_0 f(\theta) \exp\left(\frac{-E_{b,\mathrm{CH_4}}}{kT}\right) = 2.777 \times 10^{-4}\,\mathrm{s^{-1}Pa^{-1}}, \tag{51}$$

where we have approximated $f(\theta) \approx 1$.

E Attachment Kinetics

In the previous sections we have computed the kinetic laws for the deposition of CH and C, but our goal is to describe graphene growth based on the attachment of both species, as a function of $p_{\mathrm{H_2}}$. We will assume that the attaching species is either C at low $p_{\mathrm{H_2}}$ or CH, in accordance with Safron and Arnold [30].

Our main hypothesis is that C attaches to graphene when the interface is not decorated with H and CH attaches to it when the interface is decorated. With the idea of maintaining the model as simple as possible, we will take the model as a single species model, with coverage θ_{eff} and derive the effective deposition rate and the effective attachment kinetics that are consistent, with a minimal amount of further assumptions.

We begin by describing the hydrogen decoration of the edge, continue by describing the kinetics and finally, in light of the conservation of the coverage, derive the effective value of the kinetic attachment coefficient and the effective deposition rate.

E.1 Hydrogen decoration of the Step Edge

Our first assumption in order to model the system is that H_2 adsorption is selective, meaning that it is ëasier"to attach at the step edge. Then, we will have the following reaction at the step edge (where we ignore all possible attachment processes, e.g. H_2 diffusion):

$$\mathrm{H_{2(g)}} + 2\,\mathrm{S_e} \underset{k_{D,e,\mathrm{H}}}{\overset{k_{AD,e,\mathrm{H_2}}}{\rightleftharpoons}} 2\,\mathrm{H_{(e)}}, \tag{52}$$

where S_e are adsorption sites at the edge. The previous reaction results in the following equation:

$$\frac{d\theta_{\mathrm{H_{(e)}}}}{dt} = k_{AD,\mathrm{H_2}} \left[p_{\mathrm{H_2}} \left(1 - \theta_{\mathrm{H_{(e)}}}\right)^2 - K^{-1}_{\mathrm{H},(e)} \theta^2_{\mathrm{H_{(e)}}} \right]. \tag{53}$$

If we impose equilibrium, we obtain the following value for $\theta_{\mathrm{H}_{(\mathrm{e})}}$:

$$\theta_{\mathrm{H}_{(\mathrm{e})}} = \frac{\left(\frac{p_{\mathrm{H}_2}}{p_{\mathrm{H}_2,c}}\right)^{1/2}}{1+\left(\frac{p_{\mathrm{H}_2}}{p_{\mathrm{H}_2,c}}\right)^{1/2}}, \tag{54}$$

where $p_{\mathrm{H}_2,c} = K^{-1}_{\mathrm{H},(e)}$. Note that $K_{\mathrm{H},(e)}$ is unknown, although we will initially estimate it with a value that should be larger than K_{H}, the equilibrium constant at the crystal terraces. Eq. (54) is at best an approximation, as we do not know the real kinetics of this edge-attachment process for H_2.

If we accept a more general reaction order, we have:

$$\theta_{\mathrm{H}_{(\mathrm{e})}} = \frac{\left(\frac{p_{\mathrm{H}_2}}{p_{\mathrm{H}_2,c}}\right)^{2m}}{1+\left(\frac{p_{\mathrm{H}_2}}{p_{\mathrm{H}_2,c}}\right)^{2m}}, \tag{55}$$

E.2 Kinetic Coefficient

Following Pierre-Louis [27] we have the following relations in the frame of reference of an advancing step with velocity V:

$$\begin{aligned}
-(j_{+\mathrm{CH}} - j_{r,\mathrm{CH}})\cdot\hat{n} = \\
L_{+\mathrm{CH},+\mathrm{CH}}X_{+\mathrm{CH}} + L_{+\mathrm{CH},+\mathrm{C}}X_{+\mathrm{C}} + L_{+\mathrm{CH},-\mathrm{CH}}X_{-\mathrm{CH}} + L_{+\mathrm{CH},-\mathrm{C}}X_{-\mathrm{C}} \\
-(j_{+\mathrm{C}} - j_{r,\mathrm{C}})\cdot\hat{n} = \\
L_{+\mathrm{C},+\mathrm{CH}}X_{+\mathrm{CH}} + L_{+\mathrm{C},+\mathrm{C}}X_{+\mathrm{C}} + L_{+\mathrm{C},-\mathrm{CH}}X_{-\mathrm{CH}} + L_{+\mathrm{C},-\mathrm{C}}X_{-\mathrm{C}} \\
(j_{-\mathrm{CH}} - j_{r,\mathrm{CH}})\cdot\hat{n} = \\
L_{-\mathrm{CH},+\mathrm{CH}}X_{+\mathrm{CH}} + L_{-\mathrm{CH},+\mathrm{C}}X_{+\mathrm{C}} + L_{-\mathrm{CH},-\mathrm{CH}}X_{-\mathrm{CH}} + L_{-\mathrm{CH},-\mathrm{C}}X_{-\mathrm{C}} \\
(j_{-\mathrm{C}} - j_{r,\mathrm{C}})\cdot\hat{n} = \\
L_{-\mathrm{C},+\mathrm{CH}}X_{+\mathrm{CH}} + L_{-\mathrm{C},+\mathrm{C}}X_{+\mathrm{C}} + L_{-\mathrm{C},-\mathrm{CH}}X_{-\mathrm{CH}} + L_{-\mathrm{C},-\mathrm{C}}X_{-\mathrm{C}}
\end{aligned}$$

We define $X_{+\mathrm{CH}} = (\theta_{\mathrm{CH},+} - \theta_{\mathrm{CH},eq})$ on the substrate $(+)$ side and respectively for the graphene $(-)$ side (similar definitions apply to C). We define $\nu_{+\mathrm{CH}} = L_{+\mathrm{CH},+\mathrm{CH}} - \nu_{0,\mathrm{CH}}$ and $\nu_{+\mathrm{C}} = L_{+\mathrm{C},+\mathrm{C}} - \nu_{0,\mathrm{C}}$ where ν_0 is the coefficient of direct exchange between terraces, $L_{+\mathrm{CH},-\mathrm{CH}} = L_{-\mathrm{CH},+\mathrm{CH}} = -\nu_{0,\mathrm{CH}}$ and $L_{+\mathrm{C},-\mathrm{C}} = L_{-\mathrm{C},+\mathrm{C}} = -\nu_{0,\mathrm{C}}$. We disregard all other cross coefficients, assuming they correspond to a slower timescale. The resulting equations read:

$$\begin{aligned}
-(j_{+\mathrm{CH}} - j_{r,\mathrm{CH}})\cdot\hat{n} &= \nu_{+\mathrm{CH}}(\theta_{\mathrm{CH},+} - \theta_{\mathrm{CH},eq}) + \nu_{0,\mathrm{CH}}(\theta_{\mathrm{CH},+} - \theta_{\mathrm{CH},-}) \\
-(j_{+\mathrm{C}} - j_{r,\mathrm{C}})\cdot\hat{n} &= \nu_{+\mathrm{C}}(\theta_{\mathrm{C},+} - \theta_{\mathrm{C},eq}) + \nu_{0,\mathrm{C}}(\theta_{\mathrm{C},+} - \theta_{\mathrm{C},-}) \\
(j_{-\mathrm{CH}} - j_{r,\mathrm{CH}})\cdot\hat{n} &= \nu_{-\mathrm{CH}}(\theta_{\mathrm{CH},-} - \theta_{\mathrm{CH},eq}) + \nu_{0,\mathrm{CH}}(\theta_{\mathrm{CH},-} - \theta_{\mathrm{CH},+}) \\
(j_{-\mathrm{C}} - j_{r,\mathrm{C}})\cdot\hat{n} &= \nu_{-\mathrm{C}}(\theta_{\mathrm{C},-} - \theta_{\mathrm{C},eq}) + \nu_{0,\mathrm{C}}(\theta_{\mathrm{C},-} - \theta_{\mathrm{C},+})
\end{aligned}$$

If we add the left hand side of the previous system, we obtain the following:

$$(j_{-\mathrm{CH}} - j_{+\mathrm{CH}} + j_{-\mathrm{C}} - j_{+\mathrm{C}}) \cdot \hat{n} = V, \tag{56}$$

i.e. the velocity of the step

Now, assuming that $\nu_{\pm} \ll \nu_0$ (the transparency approximation), we will have that $\theta_{\mathrm{CH},+} = \theta_{\mathrm{CH},-}$ and $\theta_{\mathrm{C},+} = \theta_{\mathrm{C},-}$, which implies, by adding the right hand side of the system:

$$V = (\nu_{+\mathrm{CH}} + \nu_{-\mathrm{CH}})\,(\theta_{\mathrm{CH},\pm} - \theta_{\mathrm{CH},eq}) + (\nu_{+\mathrm{C}} + \nu_{-\mathrm{C}})\,(\theta_{\mathrm{C},\pm} - \theta_{\mathrm{C},eq}). \tag{57}$$

In the transparency limit, the distinction between ν_+ and ν_- is lost, and hence, by defining $\nu_{\mathrm{CH}} = \nu_{+\mathrm{CH}} + \nu_{-\mathrm{CH}}$ and $\nu_{\mathrm{C}} = \nu_{+\mathrm{C}} + \nu_{-\mathrm{C}}$ we have that

$$V = \nu_{\mathrm{CH}}(\theta_{\mathrm{CH},\pm} - \theta_{\mathrm{CH},eq}) + \nu_{\mathrm{C}}(\theta_{\mathrm{C},\pm} - \theta_{\mathrm{C},eq}). \tag{58}$$

Finally, we introduce our assumption of zero CH attachment in the absence of H decoration and zero C attachment when the interface is fully decorated. We can enforce this explicitly by rewriting the attachment-detachment coefficients as follows:

$$\begin{aligned} \nu_{\mathrm{CH}} &= \theta_{\mathrm{H}_{(e)}} \nu'_{\mathrm{CH}}, \\ \nu_{\mathrm{C}} &= (1 - \theta_{\mathrm{H}_{(e)}}) \nu'_{\mathrm{C}}. \end{aligned}$$

Hence,

$$V = \theta_{\mathrm{H}_{(e)}} \nu'_{\mathrm{CH}}(\theta_{\mathrm{CH},\pm} - \theta_{\mathrm{CH},eq}) + (1 - \theta_{\mathrm{H}_{(e)}}) \nu'_{\mathrm{C}}(\theta_{\mathrm{C},\pm} - \theta_{\mathrm{C},eq}). \tag{59}$$

Now, we define the effective species kinetic coefficient through Eq. (59):

$$\begin{aligned} \beta_{eff} V = \theta_{eff} - \theta_{eff,eq} = \\ \beta_{eff} \left[\theta_{\mathrm{H}_{(e)}} \nu'_{\mathrm{CH}}(\theta_{\mathrm{CH},\pm} - \theta_{\mathrm{CH},eq}) + (1 - \theta_{\mathrm{H}_{(e)}}) \nu'_{\mathrm{C}}(\theta_{\mathrm{C},\pm} - \theta_{\mathrm{C},eq}) \right]. \end{aligned} \tag{60}$$

E.3 Flux Consistency

If we define θ_{eff} as a linear combination of the coverages of C and CH,

$$\theta_{eff} = \alpha_{\mathrm{CH}} \theta_{\mathrm{CH}} + \alpha_{\mathrm{C}} \theta_{\mathrm{C}} \tag{61}$$

we have an additional condition on the admisible combinations, derived from conservation of the coverage.

By the definition of normal flux, at the interface (negative implies incoming flux, into a small Gaussian pillbox):

$$j_{n,eff,\pm} = \mp\, \hat{n} \cdot D_{eff} \nabla \theta_{eff}|_{\pm} \mp V \theta_{eff,\pm}, \tag{62}$$

where $\hat{n}$ is the interface normal, from the $-$ side to the $+$ side.

The conservation of θ_{eff} and the transparency approximation imply the following:

$$j_{n,eff,+} + j_{n,eff,-} = \hat{n} \cdot D_{eff} \left(\nabla \theta_{eff}|_{-} - \nabla \theta_{eff}|_{+} \right) = -V. \tag{63}$$

Now, we can investigate whether θ_{eff} is in effect conserved and what is the value of D_{eff}.

To check the consistency of the approach, we can break down the flux as C flux and CH flux, by using the definition of θ_{eff}. We ignore the values at the boundary as we know that they would eventually cancel when finding the jump condition:

$$\begin{aligned} j_{n,eff,\pm} = &\mp \hat{n} \cdot D_{eff}\alpha_{\mathrm{CH}}\nabla\theta_{\mathrm{CH}}|_{\pm} \mp \hat{n} \cdot D_{eff}\alpha_{\mathrm{C}}\nabla\theta_{\mathrm{C}}|_{\pm} \\ &\mp V\left(\alpha_{\mathrm{CH}}\theta_{\mathrm{CH},\pm} + \alpha_{\mathrm{C}}\theta_{\mathrm{C},\pm}\right). \end{aligned} \tag{64}$$

Ignoring cross-diffusion effects, If we take the diffusion coefficient of C and CH as D, then we can write the jump condition as follows:

$$j_{n,eff,+} + j_{n,eff,-} = \frac{D_{eff}}{D}\alpha_{\mathrm{CH}}\left(j_{n,\mathrm{CH},+} + j_{n,\mathrm{CH},-}\right) + \frac{D_{eff}}{D}\alpha_{\mathrm{C}}\left(j_{n,\mathrm{C},+} + j_{n,\mathrm{C},-}\right). \tag{65}$$

Global conservation of coverage implies that

$$j_{n,\mathrm{CH},+} + j_{n,\mathrm{CH},-} + j_{n,\mathrm{C},+} + j_{n,\mathrm{C},-} = -V, \tag{66}$$

but this condition alone does not allow us to recover Eq. (63).

Going back to equation (65), we see that it is consistent with (66) only if $\alpha_{\mathrm{CH}} = \alpha_{\mathrm{C}} = \alpha$ and $D_{eff} = D/\alpha$. In other words, what is conserved is the coverage.

By setting $\alpha = 1$ so that $D_{eff} = D$, we obtain that $\theta_{eff} = \theta_{\mathrm{CH}} + \theta_{\mathrm{C}}$, and kinetics depending on the concentration at the interface. Explicitly, from Eq. (60):

$$\beta_{eff} = \frac{\theta_{\mathrm{CH},\pm} + \theta_{\mathrm{C},\pm} - \theta_{\mathrm{CH},eq} - \theta_{\mathrm{C},eq}}{\theta_{\mathrm{H}_{(e)}}\nu'_{\mathrm{CH}}\left(\theta_{\mathrm{CH},\pm} - \theta_{\mathrm{CH},eq}\right) + (1-\theta_{\mathrm{H}_{(e)}})\nu'_{\mathrm{C}}\left(\theta_{\mathrm{C},\pm} - \theta_{\mathrm{C},eq}\right)}. \tag{67}$$

E.4 Additional Assumptions

While Eq. (67) is very complicated, a single assumption puts it in a very simple form. This assumption is that Eq. (23) is also valid close to the step edge, its equilibration is fast enough and hence $\theta_{\mathrm{C},\pm} \propto \theta_{\mathrm{CH},\pm}$. Explicitly, considering $\theta_{\mathrm{C},\pm}, \theta_{\mathrm{CH},\pm} \ll 1$:

$$\theta_{\mathrm{C},\pm} = K_{3,(e)}\left(\frac{1}{\theta_{\mathrm{H}_{(e)}}} - 1\right)\theta_{\mathrm{CH},\pm}, \tag{68}$$

where $K_{3,(e)}$ is the analogue of K_3 close to the edge.

With the previous result, we can rewrite Eq. (67) as follows:

$$\beta_{eff} = \frac{\theta_{\mathrm{H}_{(e)}} + \left(1-\theta_{\mathrm{H}_{(e)}}\right)K_{3,(e)}}{\theta^2_{\mathrm{H}_{(e)}}\nu'_{\mathrm{CH}} + \left(1-\theta_{\mathrm{H}_{(e)}}\right)^2\nu'_{\mathrm{C}}K_{3,(e)}}. \tag{69}$$

Then, using Eq. (55) we obtain:

$$\beta_{eff}\nu'_{\mathrm{C}} = \frac{\left(\frac{p_{\mathrm{H}_2}}{p_{\mathrm{H}_2,c}}\right)^{2m} + K_{3,(e)}}{\left(\frac{p_{\mathrm{H}_2}}{p_{\mathrm{H}_2,c}}\right)^{4m}\frac{\nu'_{\mathrm{CH}}}{\nu'_{\mathrm{C}}} + K_{3,(e)}}\left[1 + \left(\frac{p_{\mathrm{H}_2}}{p_{\mathrm{H}_2,c}}\right)^{2m}\right]. \tag{70}$$

The previous expression has a maximum for the following value of the pressure:

$$p^{2m}_{\mathrm{H}_2} = p^{2m}_{\mathrm{H}_2,c}\frac{K_{3,(e)}\left(1 - \frac{\nu'_{\mathrm{CH}}}{\nu'_{\mathrm{C}}}\right) + \sqrt{K_{3,(e)}\left(K_{3,(e)} + \frac{\nu'_{\mathrm{CH}}}{\nu'_{\mathrm{C}}}\right)\left(K_{3,(e)}\frac{\nu'_{\mathrm{CH}}}{\nu'_{\mathrm{C}}} + 1\right)}}{\frac{\nu'_{\mathrm{CH}}}{\nu'_{\mathrm{C}}}\left(K_{3,(e)} + 1\right)}. \tag{71}$$

And has a finite value for $p_{\mathrm{H}_2} \to 0$, $\beta_{eff}\nu'_{\mathrm{C}} = 1$, as expected. If we assume that carbon attachment is unlikely, then $\nu'_{\mathrm{C}} \to 0$ and we have that:

$$\beta_{eff}\nu'_{\mathrm{CH}} \approx 1 + K_{3,(e)}\left(\frac{p_{\mathrm{H}_2}}{p_{\mathrm{H}_2,c}}\right)^{-4m} \tag{72}$$

where we have taken into account that, in general $p_{\mathrm{H}_2}/p_{\mathrm{H}_2,c} \ll 1$. Note how, even though it is assumed to be small, the leading order term is multiplied by $K_{3,(e)}$. Using this formula does not alter substantially the observed results.

F Alternative Values of the Kinetic Parameters

While in the main text we have only considered the case $m = 1$, we have also explored other possible values of the order of reaction m in Eq. (55). In addition, we have investigated the effect of nonlinearity in the attachment of CH:

$$V = \theta^n_{\mathrm{H}_{(e)}}\nu'_{\mathrm{CH}}(\theta_{\mathrm{CH},\pm} - \theta_{\mathrm{CH},eq}) + (1 - \theta_{\mathrm{H}_{(e)}})\nu'_{\mathrm{C}}(\theta_{\mathrm{C},\pm} - \theta_{\mathrm{C},eq}), \tag{73}$$

where we have taken $n = 1$ in the main text. Note that there could be another nonlinearity in the attachment of C but we do not take it into account given the relation $\nu'_{\mathrm{CH}}/\nu'_{\mathrm{C}} \gg 1$. In all cases, we obtain results similar to those shown in the present paper.

G Summary

Putting everything together, we have a model of the following form:

$$\partial_t\theta_{eff} = \nabla\cdot(D_{eff}\nabla\theta_{eff}) + F_{eff}, \tag{74a}$$

$$V = \hat{n}\cdot D_{eff}\left(\nabla\theta_{eff}|_+ - \nabla\theta_{eff}|_-\right), \tag{74b}$$

$$\beta_{eff}V = \theta_{eff} - \theta_{eff,eq}, \tag{74c}$$

where $D_{eff} = D_{\mathrm{C}} = D_{\mathrm{CH}}$, $\theta_{eff} = \theta_{\mathrm{C}} + \theta_{\mathrm{CH}}$, $F_{eff} = F_{\mathrm{C}} + F_{\mathrm{CH}}$ and

$$\beta_{eff}\nu'_{\mathrm{C}} = \frac{\left(\frac{p_{\mathrm{H}_2}}{p_{\mathrm{H}_2,c}}\right)^{2m} + K_{3,(e)}}{\left(\frac{p_{\mathrm{H}_2}}{p_{\mathrm{H}_2,c}}\right)^{4m} \frac{\nu'_{\mathrm{CH}}}{\nu'_{\mathrm{C}}} + K_{3,(e)}} \left[1 + \left(\frac{p_{\mathrm{H}_2}}{p_{\mathrm{H}_2,c}}\right)^{2m}\right], \tag{74d}$$

where ν'_{C} is the kinetic attachment-detachment coefficient of C to graphene at zero hydrogen edge coverage and ν'_{CH} is the attachment-detachment coefficient of CH for a fully hydrogen-decorated edge.

Next, we define the parameters for the BCF and phase field models presented in the main text. From the definition in the main text we obtain that

$$f_{eff} = \frac{l^2\Omega}{D}\left(F_{\mathrm{C}} + F_{\mathrm{CH}}\right) = \frac{l^2\Omega}{D} F_{eff,pre}\left(\frac{K_3}{\sqrt{K_{\mathrm{H}}}p_{\mathrm{H}_2}^{3/2}} + \frac{1}{p_{\mathrm{H}_2}}\right), \tag{75}$$

where

$$F_{eff,pre} = \frac{p_{\mathrm{CH}_4} K_1 K_2 k_{AD,\mathrm{CH}_4}}{\Omega K_{\mathrm{H}}}, \tag{76}$$

and D are computed so that $f_{eff}|_{p_{\mathrm{H}_2}=1250\mathrm{Pa}}$ corresponds to a shape similar to the ones found in Vlassiouk et al. [33], its value is given in Table 1. This fixes our timescale and it is well within the range of possible values of D discussed above.

From Eq. (6) we obtain that

$$\beta_{eff} = \frac{\left(K_{\mathrm{H},(e)}^2 p_{\mathrm{H}_2}^2 + 1\right)\left(K_{3,(e)} + K_{\mathrm{H},(e)}^2 p_{\mathrm{H}_2}^2\right)}{\nu'_{\mathrm{C}}\left(K_{3,(e)} + K_{\mathrm{H},(e)}^4 K_{kin} p_{\mathrm{H}_2}^4\right)}, \tag{77}$$

where $K_{kin} = \nu'_{\mathrm{CH}}/\nu'_{\mathrm{C}}$, its value is defined in Table 1.

Since ν'_{C} is unknown, we rescale β_{eff} so that at its peak it has a reference value corresponding to the one found in Meca et al. [24].

$$\tilde{\beta}_{eff} = \beta_0 \frac{\beta_{eff}}{\beta_{eff}|_{p_{\mathrm{H}_2}=1250\mathrm{Pa}}}. \tag{78}$$

Note that the previous values are non-dimensional. See [24] and the discussion therein on its value. In order to obtain this value of the kinetic parameter, parameter α in Eq. (13) has to be defined as:

$$\alpha = \frac{\lambda\sqrt{2}}{20}\tilde{\beta}_{eff}, \tag{79}$$

where λ, the other phase-field parameter, is defined as $\lambda = 10\sqrt{2}/d_0$ where d_0 is the capillary parameter. The value given in Table 7 implies a capillary length of $d_0 l = 6 \times 10^{-10}$m.

Paramenter	*Symbol*	*Value*
Reference Kinetic Coefficient	β_0	5.54×10^{-3}
Capillary parameter	d_0	6×10^{-4}
Interface width	ϵ	2.5×10^{-3}
Kinetic anisotropy	$\epsilon_{k,6}$	0.08
Edge energy anisotropy	$\epsilon_{e,6}$	10^{-3}
Dimensional length	l	10^{-6}m
Prefactor for F_{eff}	$F_{eff,pre}$	7.31×10^{19}m^{-2}s^{-1}Pa

Table 7: Additional parameters needed for the numerical solution of the Phase-Field model. All parameters are defined as in Meca et al. [24], except for $F_{eff,pre}$, which is computed using Table 1.

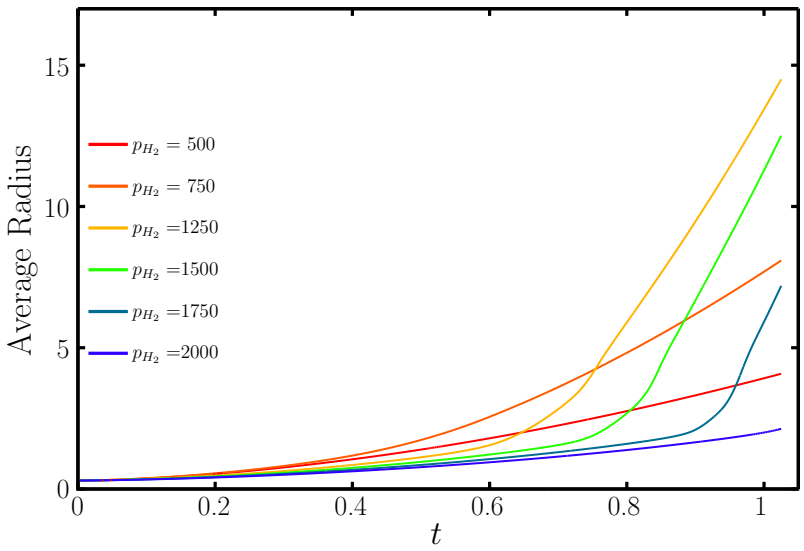

Figure 6: Evolution of the average radius of the crystallites as a function of time. Case $n = 1$, $m = 1$.

H Additional figures

Fig. 6 includes more curves with the evolution of the average radius than Fig. 2. They can be compared with those from Fig. 7, that features the solution curves of Eq. (11). Additionally, Fig. 7 displays a fit to Eq. (12) where we allow $r(0)$ to depend on p_{H_2}, as opposed to the fits shown in Fig. 4.

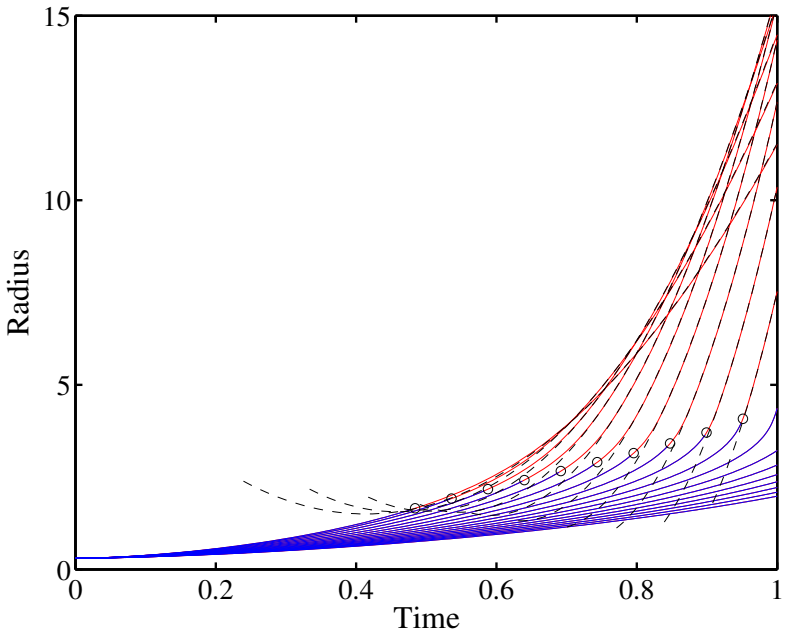

Figure 7: Growth curves obtained from the boundary integral (Eq. 11). The red color represents the kinetics-controlled regime, while the blue is the diffusion-controlled regime. Dashed curves correspond to a one-parameter ($r(0)$) fit to Eq. (12).